Supporting Information

Chiral Shape Engineering Combined with Bimetallic Nanostructures for High-Performance Plasmonic Sulfide Sensors

Han Lin[ab], Kuniharu Ijiro[b], Hideyuki Mitomo[bc]*

a. Graduate School of Life Science, Hokkaido University, Kita 10, Nishi 8, Kita-Ku, Sapporo 060-0810, Japan

b. Research Institute for Electronic Science, Hokkaido University, Kita 21, Nishi 10, Kita-Ku, Sapporo 001-0021, Japan

c. Institute of Multidisciplinary Research for Advanced Materials, Tohoku University, Sendai 980-8577, Japan

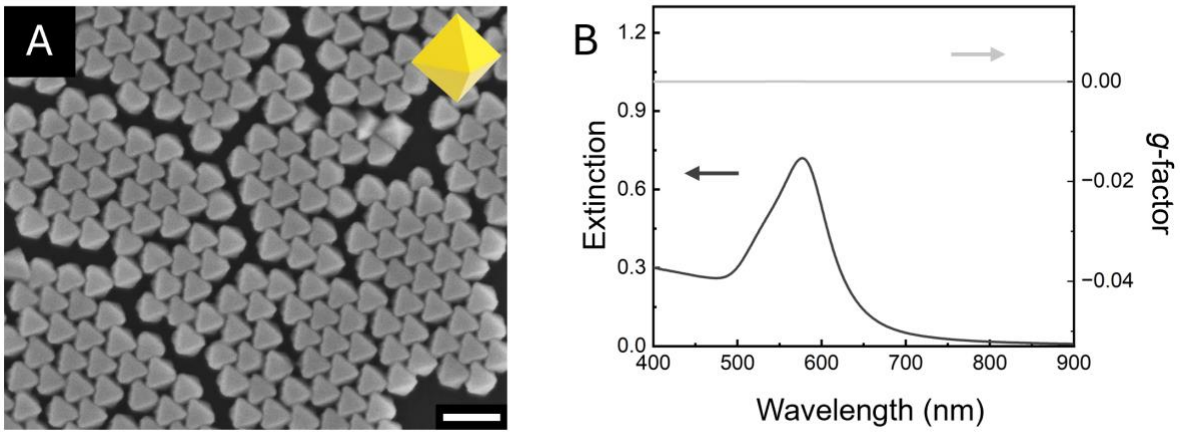

Figure S1. Characteristics of Au octahedral nanoparticles (Au ONPs). (A) SEM image of the Au ONPs, the inset shows a schematic illustration. (B) Extinction and *g*-factor spectra of Au ONPs. The scale bar is 100 nm.

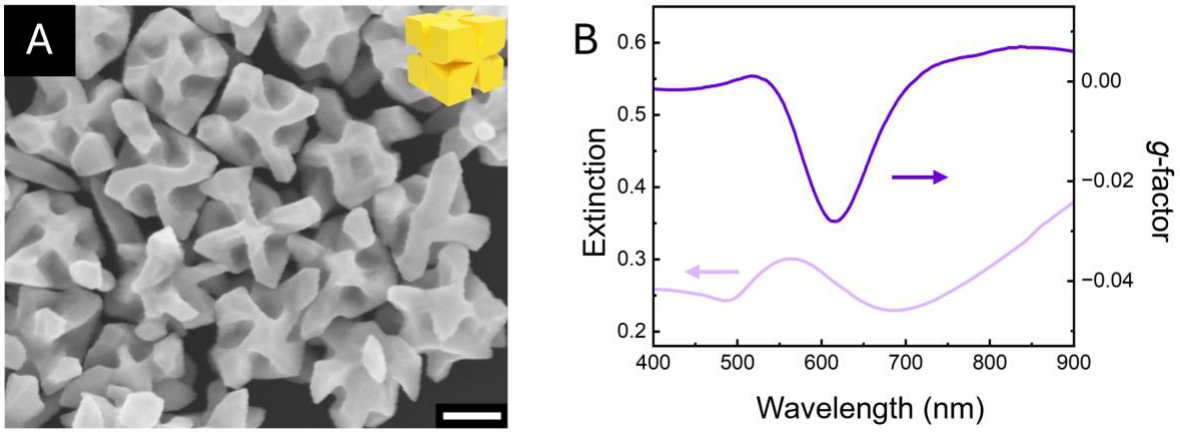

Figure S2. Characteristics of chiral Au nanoparticles (c-Au NPs). (A) SEM image of the c-Au NPs, the inset shows a schematic illustration. (B) Extinction and *g*-factor spectra of c-Au NPs. The scale bar is 100 nm.

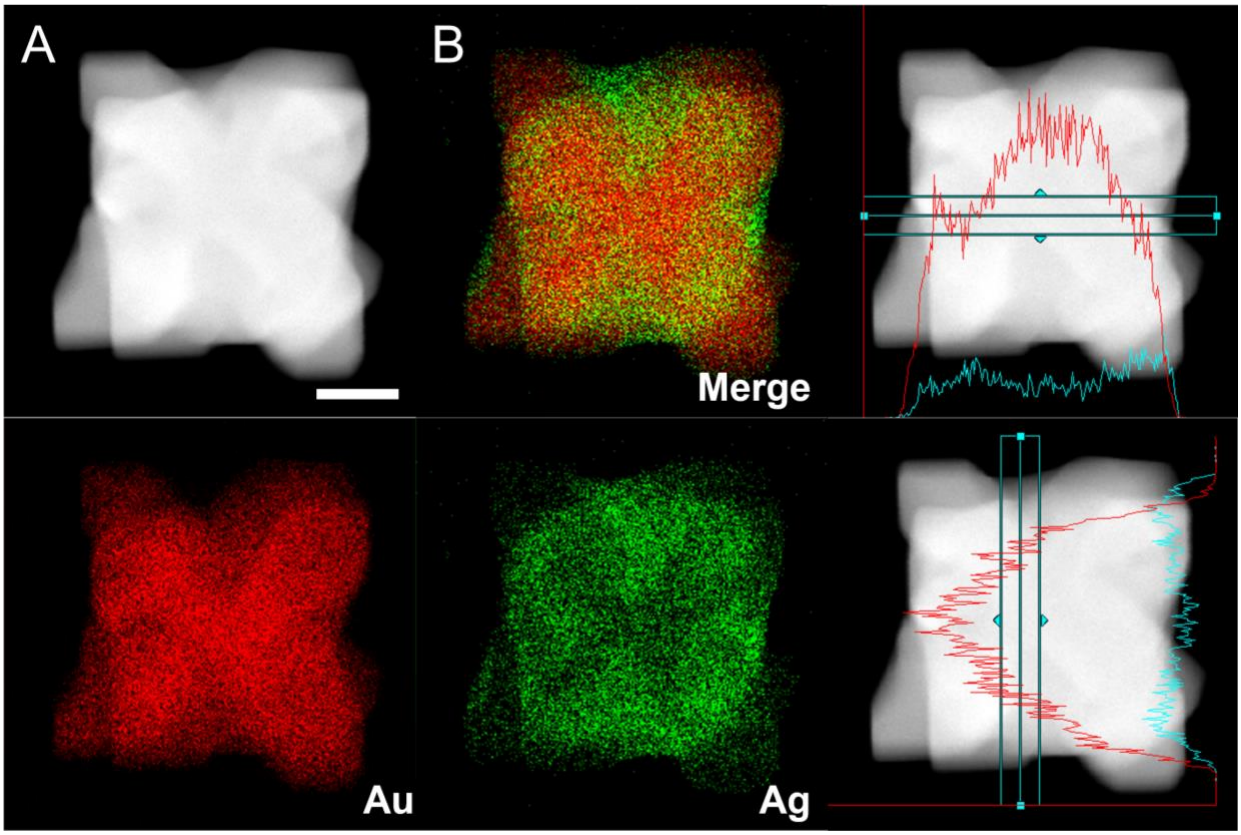

Figure S3. (A) HAADF-STEM image and (B-F) corresponding EDS mapping images of c-Au@Ag NPs (iv). The scale bar represents 50 nm.

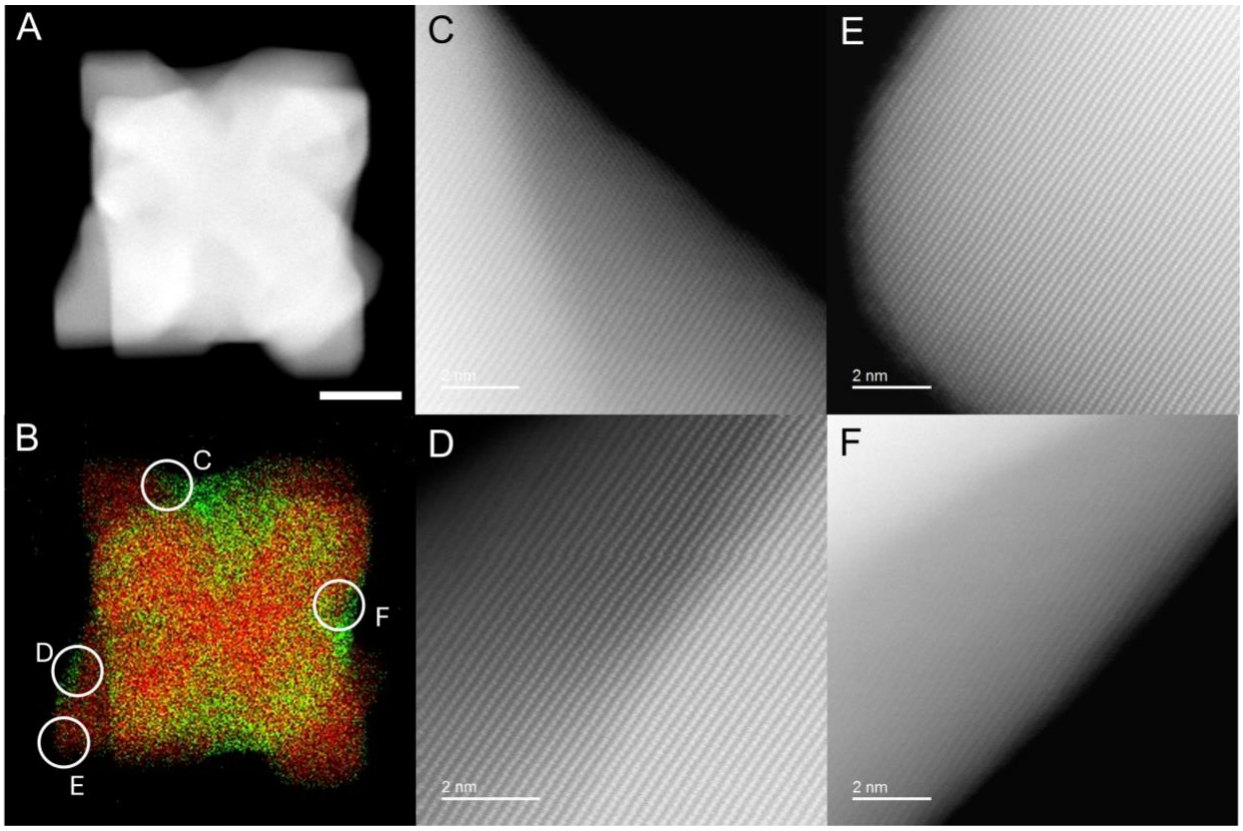

Figure S4. (A) HAADF-STEM image and (B) corresponding EDS mapping image of c-Au@Ag NPs (iv). The scale bar represents 50 nm. (C-F) HRTEM images of four sites of c-Au@Ag NPs (iv).

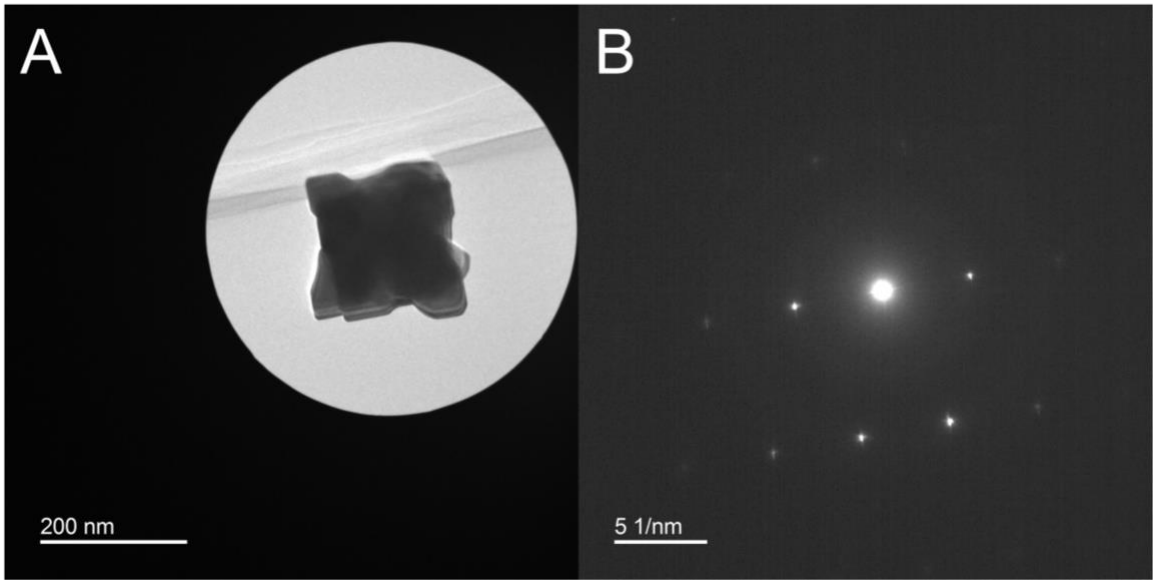

Figure S5. (A) TEM image and (B) corresponding diffraction image of c-Au@Ag NPs (iv).

Figure S6. The digital photograph of c-Au NPs and c-Au@Ag NPs colloidal solutions with different silver contents (from i to iv, the final concentrations of Ag were 30, 60, 120 and 180 μM, respectively).

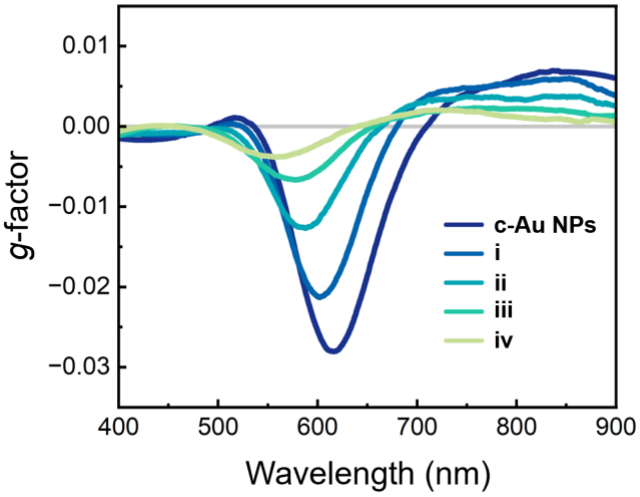

Figure S7. *g*-factor spectra of c-Au NPs and c-Au@Ag NPs with different Ag contents (from i to iv, the final concentrations of Ag were 30, 60, 120 and 180 μM, respectively).

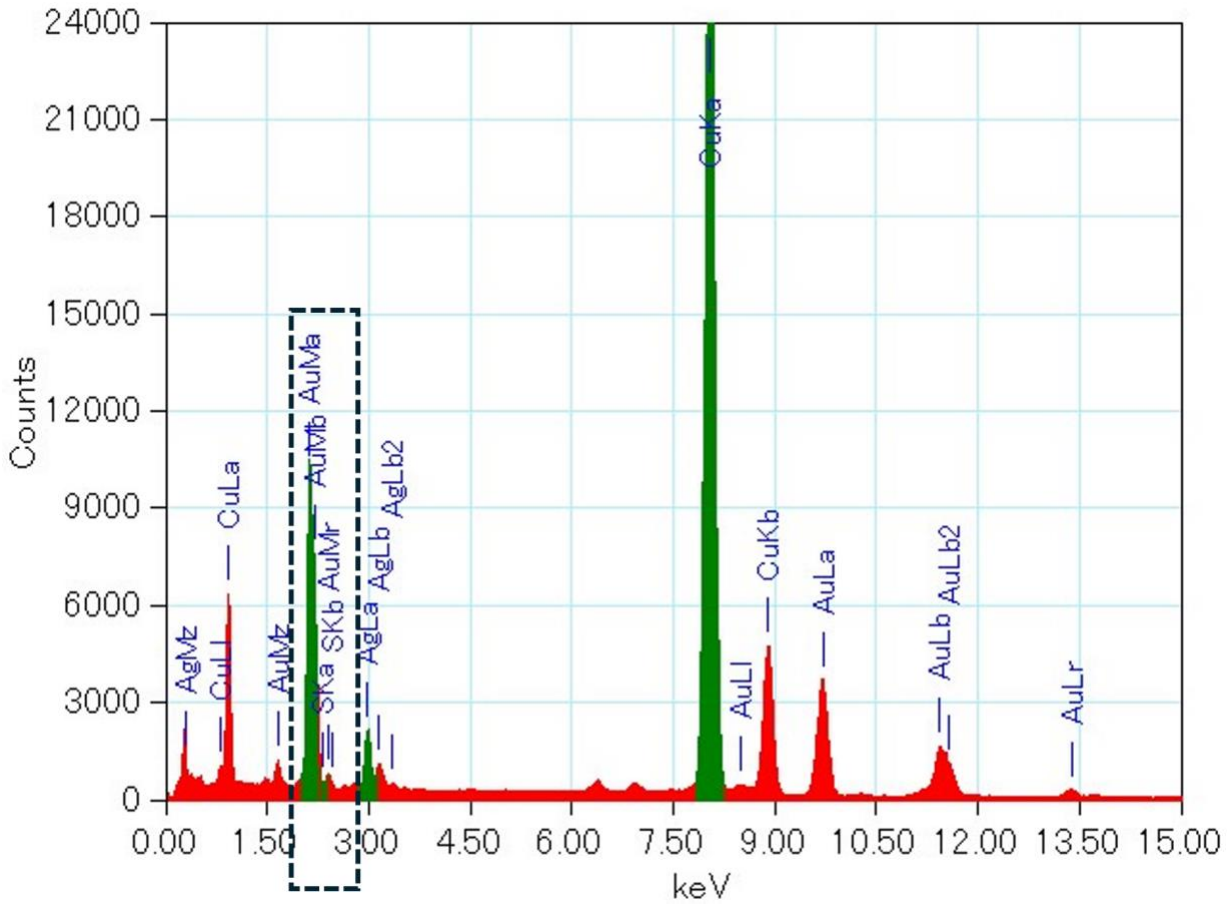

Figure S8. EDS analysis of c-Au@Ag NPs (iv).

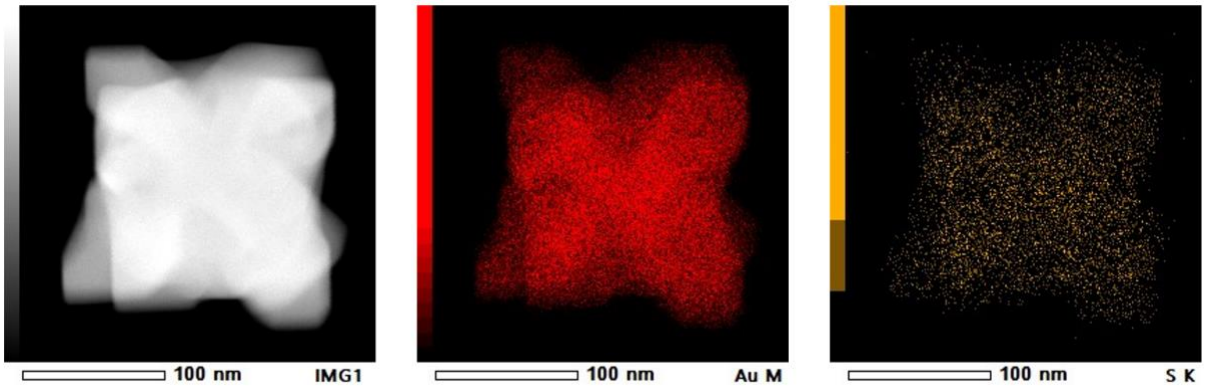

Figure S9. STEM image and corresponding EDS mapping images of c-Au@Ag NPs (iv).

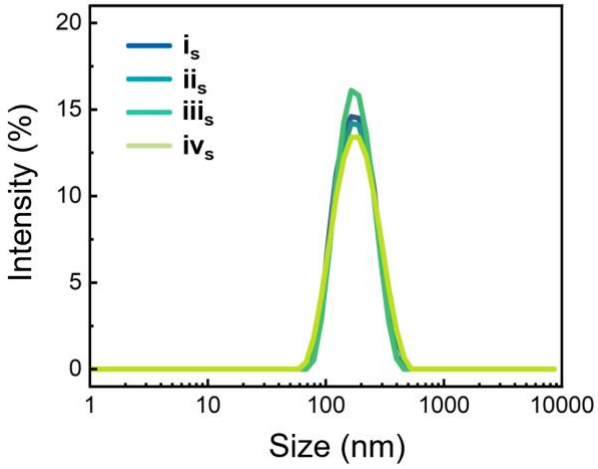

Figure S10. DLS of c-Au@Ag_2S NPs (i_s, ii_s, iii_s and iv_s).

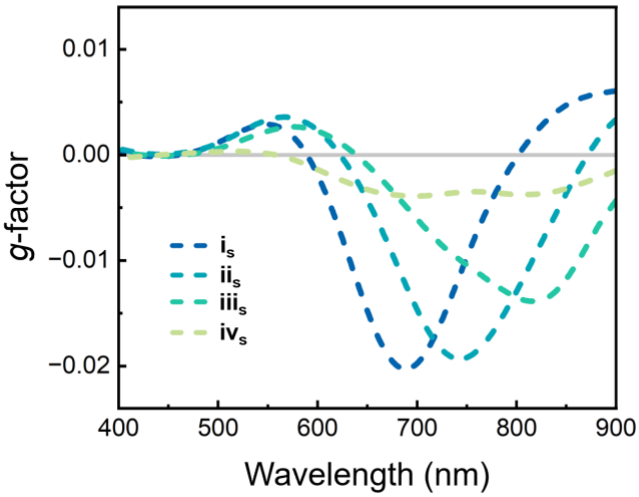

Figure S11. *g*-factor spectra of c-Au@Ag_2S NPs (i_s, ii_s, iii_s and iv_s).

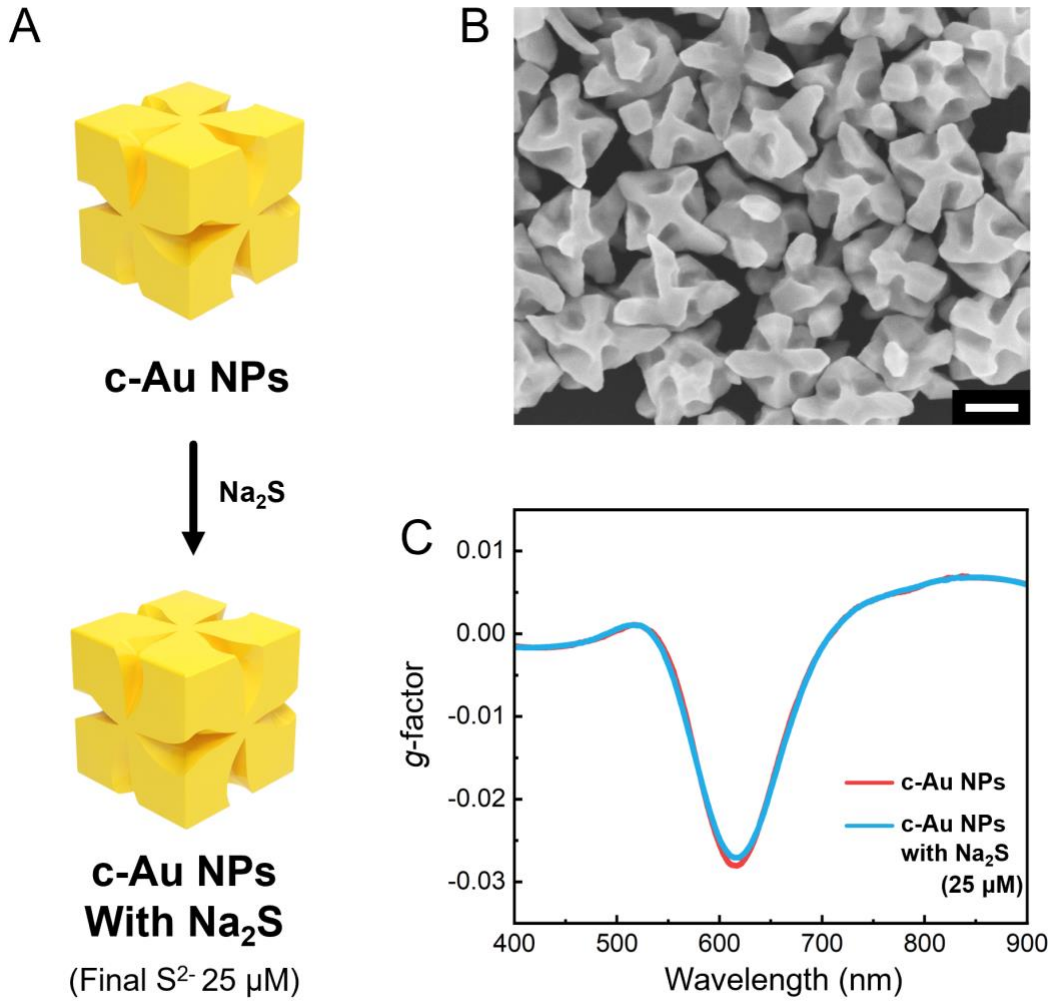

Figure S12. The importance of the Ag layer for sulfide sensing. (A) Schematic illustration and SEM image of c-Au NPs incubation in a sulfide ion (25 μM) environment. (C) *g*-factor spectra of c-Au NPs before and after incubation in a sulfide ion (25 μM) environment. The scale bar is 100 nm.

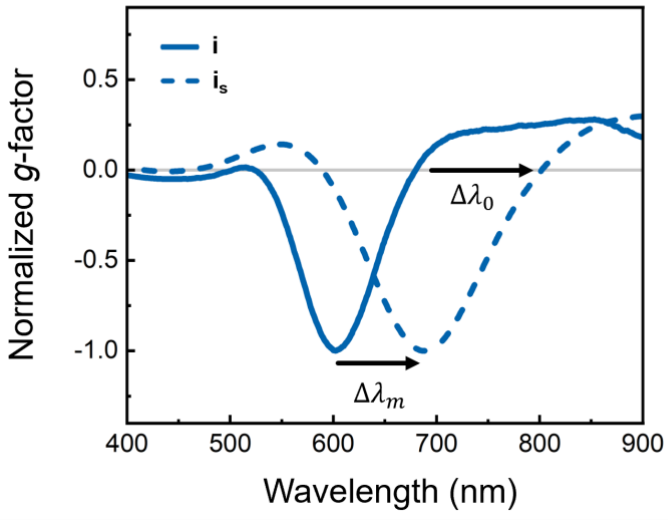

Figure S13. Normalized *g*-factor spectra of c-Au@Ag NPs before (i) and after (i_s) sulfuration.

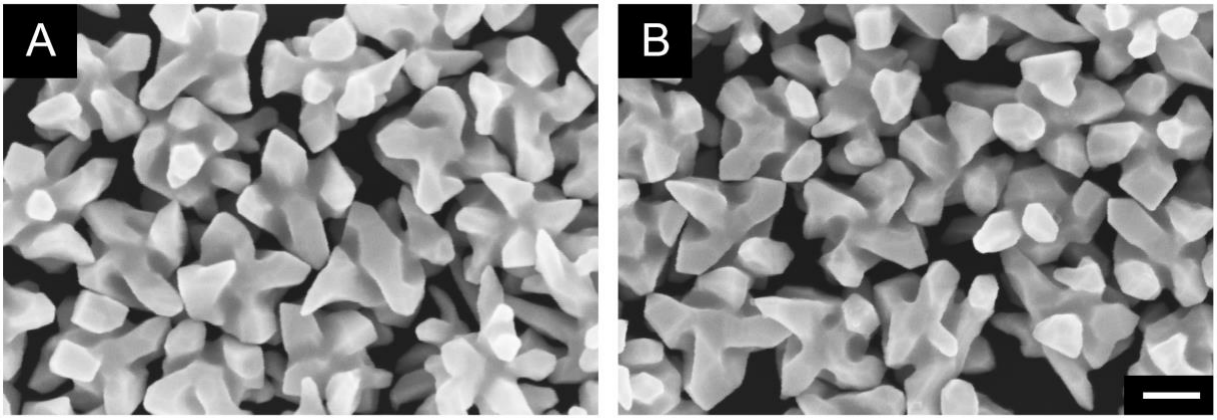

Figure S14. SEM images of c-Au@Ag_2S NPs after incubation with sulfide ion concentrations of 0.1 μM (A), 0.5 μM (B). The scale bars are 100 nm.

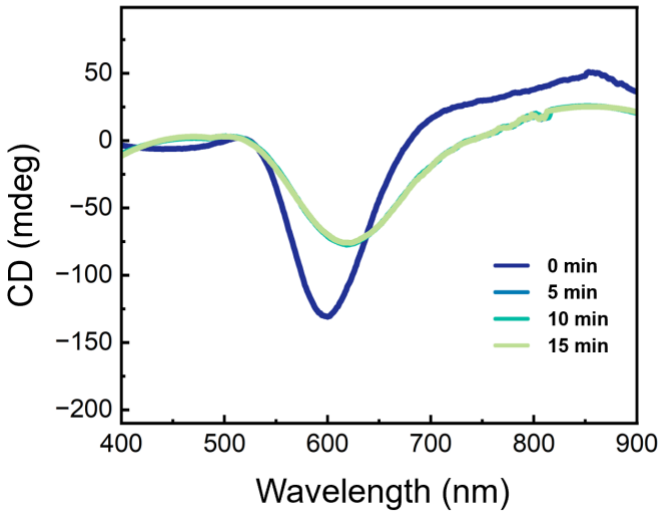

Figure S15. CD spectra of c-Au@Ag NPs and after incubation in a sulfide ion environment (2.5 μM) for 5, 10, and 15 min.

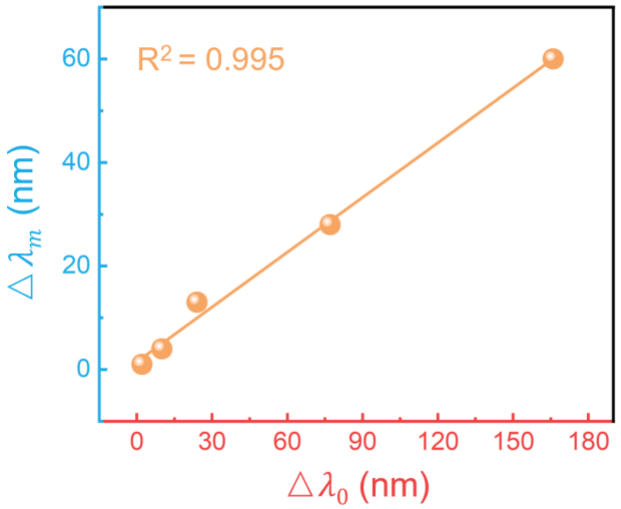

Figure S16. The correlation between the peak shifts ($\Delta\lambda_m$) and the zero-crossing point shifts ($\Delta\lambda_0$) in the CD spectra at the same sulfide concentration.

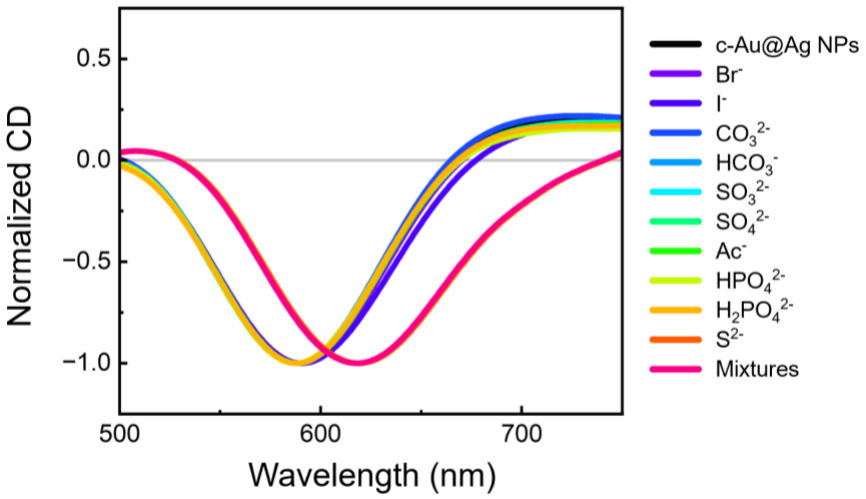

Figure S17. Normalized CD spectra of c-Au@Ag NPs after incubation in environments with sulfide ions (2.5 μM), other interfering ions (25 μM) and their mixtures (sulfide ions at 2.5 μM and all the aforementioned interfering ions at 25 μM).

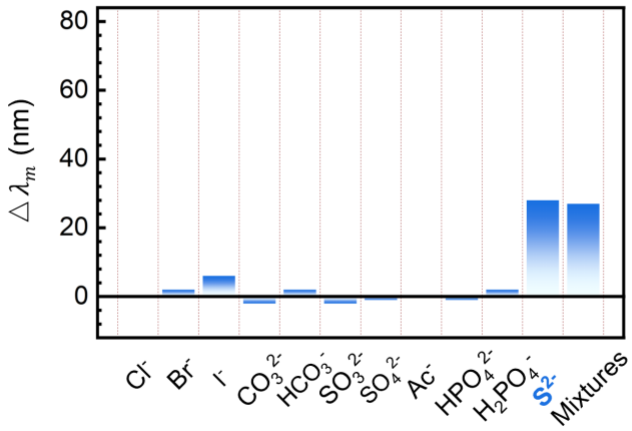

Figure S18. The CD peak shifts ($\Delta\lambda_m$) of c-Au@Ag NPs after incubation in the presence of sulfide ions (2.5 μM), other interfering ions (25 μM) and their mixtures (sulfide ions at 2.5 μM and all the aforementioned interfering ions at 25 μM).

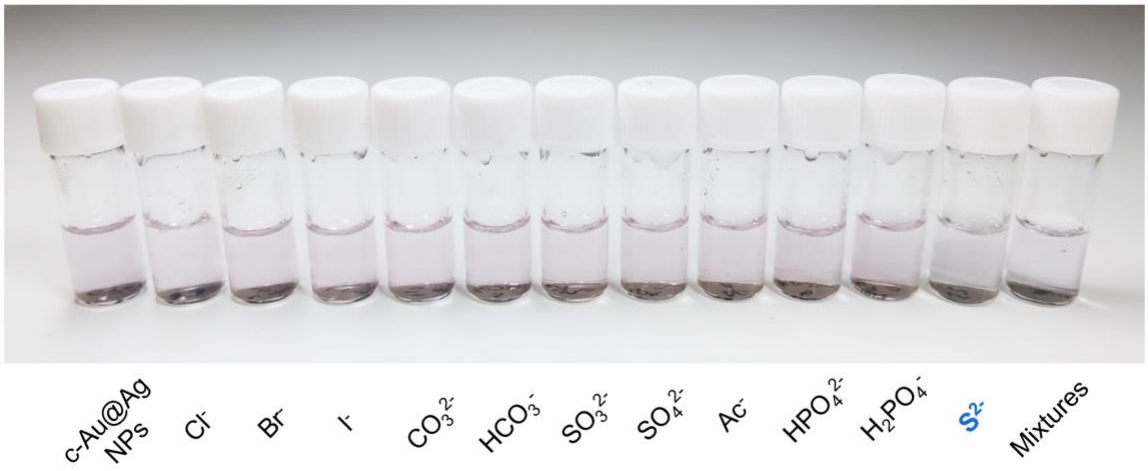

Figure S19. The digital photograph of c-Au@Ag NPs after incubation in environments with sulfide ions (2.5 μM), other interfering ions (25 μM) and their mixtures (sulfide ions at 2.5 μM and all the aforementioned interfering ions at 25 μM).